electronics

Article

A Novel Three-Dimensional Positioning Method for Foot-Mounted Pedestrian Navigation System Using Low-Cost Inertial Sensor

Dongpeng Xie [1], Jinguang Jiang [2,*], Peihui Yan [2], Jiaji Wu [2], Yuying Li [2] and Ziyan Yu [3]

1 Electronic Information School, Wuhan University, No. 129 Luoyu Road, Wuhan 430079, China
2 GNSS Research Center, Wuhan University, No. 129 Luoyu Road, Wuhan 430079, China
3 School of Computer Science, Wuhan University, No. 129 Luoyu Road, Wuhan 430079, China
* Correspondence: jinguang@whu.edu.cn

Abstract: Aiming at the problem that position errors accumulate rapidly in foot-mounted pedestrian navigation systems using a low-cost inertial sensor, a novel three-dimensional (3D) positioning method is proposed. First, when the foot is still, an improved zero velocity detection method that assigns different weights to each inertial measurement unit (IMU) data in a sliding window is designed to reduce positioning errors. When the foot is in swing, a lateral velocity restriction method is proposed by analyzing the gait characteristics of pedestrians. In addition, when pedestrians need altitude positioning in the building, the stair step height is also applied to the zero-velocity update (ZUPT)-aided inertial navigation system, which can effectively improve altitude positioning accuracy. Experiments under multi-gait modes show that the proposed zero velocity detection method can achieve smaller positioning errors compared with other traditional zero velocity detection methods. Moreover, the trajectory estimated by the proposed method has a higher coincidence with the real trajectories, the two-dimensional (2D) plane positioning error is less than 0.9% and the average altitude positioning error is only 0.12 m.

Keywords: pedestrian navigation system; three-dimensional positioning; lateral velocity restriction algorithm; stair step height; gait characteristics

check for updates

Citation: Xie, D.; Jiang, J.; Yan, P.; Wu, J.; Li, Y.; Yu, Z. A Novel Three-Dimensional Positioning Method for Foot-Mounted Pedestrian Navigation System Using Low-Cost Inertial Sensor. *Electronics* **2023**, *12*, 845. https://doi.org/10.3390/electronics12040845

Academic Editor: Arturo de la Escalera Hueso

Received: 29 December 2022
Revised: 27 January 2023
Accepted: 30 January 2023
Published: 8 February 2023

1. Introduction

Nowadays, the pedestrian navigation system (PNS) is widely used in military and civil scenarios [1–3]. Some common positioning technologies such as the Global Navigation Satellite System (GNSS) [4], Wireless Fidelity (WIFI) [5], Bluetooth [6], ZigBee [7], and Wireless Sensor Network (WSN) [8,9] can provide pedestrian positioning.Compared with the other four methods mentioned above, the PNS(INS) based on an inertial measurement unit (IMU) has attracted extensive attention due to its complete autonomy [10]. However, due to the high noise of the IMU, the positioning error of the inertial navigation system (INS) will accumulate rapidly with time [11]. In order to reduce error accumulation, in Refs. [12–14], the IMU is installed on the foot, and a zero velocity update algorithm (ZUPT) is proposed to fuse INS when the foot touches the ground. Once the foot touches the ground, the error between calculated velocity and actual velocity can be regarded as an observation to reduce the velocity error through Kalman filtering. In the ZUPT-aided PNS, a zero velocity detection algorithm is closely related to a ZUPT algorithm, the false detection in zero velocity interval will increase position error, so an effective and accurate zero velocity detection method is necessary. At present, the proposed zero velocity detectors are mainly divided into two types: the threshold detection and artificial intelligence (AI) detection. The traditional zero velocity detection methods mainly detect pedestrian gait based on the output of the gyroscope and acceleration in a time window, including angular rate measurement energy detection (AME), accelerometer measurements variance detection (AMV), accelerometer measurements magnitude detection (MAG), generalized likelihood ratio test (GLRT) and combination of above zero velocity detection methods [15–17]. The most common is a zero velocity detection based on GLRT, which can have good performance in some low velocity motion modes. Compared to these traditional zero velocity detectors, some detectors using artificial intelligence (AI) have also been proposed to achieve satisfactory performance in different gait patterns. In Ref. [18], Park et al. designed a zero velocity detector based on a hidden Markov model (HMM) and combined a heuristic heading reduction algorithm to track pedestrian position. Wagstaff et al. applied Long Short Term Memory (LSTM) to detect the zero velocity range of pedestrian movement status, and the experimental results verify that the positioning error is effectively decreased by over 34% compared to conventional zero velocity detectors with a fixed threshold [19]. Zhao et al. designed a zero velocity detector based on LSTM and used a sliding detection method to correct the pseudo zero velocity interval [20]. However, a zero velocity detection model requires high computational complexity and requires a lot of data to train. In a ZUPT-aided PNS, ZUPT cannot eliminate all the position errors, and the unobserved azimuth misalignment angle will cause the rapid accumulation of system position errors [21,22]. In recent years, some scholars have used different additional sensors to assist INS. In Ref. [23], Li et al. proposed an integration structure based on DR/WiFi fingerprinting/magnetic matching, which used low cost sensors in smart devices and WiFi infrastructures to control the position errors in the range of 13.3 to 55.2% under four motion conditions. Zeng et al. proposed an indoor/outdoor pedestrian positioning scheme based on GNSS and magnetic sensors [24], and experimental results show that the proposed method effectively improves the reliability and continuity of positioning accuracy. In Ref. [25], Ji et al. proposed an improved GLRT method to improve the accuracy of zero velocity interval detection by introducing barometer information, meanwhile, an improved algorithm combining an extended Kalman filter (EKF) and particle filter is also designed to solve the pedestrian three-dimensional (3D) positioning problem. Although these methods can achieve better performance, the use of additional sensors not only increases the hardware cost of the system but also increases the computational complexity.

In this paper, a novel 3D positioning scheme without additional sensors is proposed. For a normal gait cycle, a novel zero velocity detection method using IMU data is designed to detect zero velocity intervals. This method assigns different weights to the IMU data at different times in a time window, the weight of each IMU data sample is composed of static weight and dynamic weight. Static weight can ensure that each data sample in a time window can determine the current gait state, and the exponential distribution of dynamic weight determines that the impact of each data sample on the current state is different. In order to meet human multi-gait requirements, different threshold values are set according to the pedestrian's gait velocity. When the foot is in the non-zero velocity interval, the lateral velocity of the foot is almost zero, so according to this assumption, a lateral velocity restrict algorithm is used to improve positioning accuracy. Finally, as for the 3D positioning needs of pedestrians, the altitude change of INS in a short time can accurately measure the change in the number of steps, and the stair step height of the building is also used to assist the INS.

The remainder of this paper consists of the following parts: Section 2 shows the ZUPT-aided INS, and Section 3 studies the improved zero-velocity detection algorithm, and lateral velocity restrict algorithm. Section 4 shows the specific experimental methods and results. The last section concludes this paper.

Notations: Bold letters represent vectors or matrices, $(\boldsymbol{A})\times$ denotes the skew-symmetric matrix of matrix $\boldsymbol{A}$, $\boldsymbol{a_i}$ represents the ith element of vector $\boldsymbol{a}$, $\boldsymbol{A^T}$ denotes the transpose of matrix $\boldsymbol{A}$, $\boldsymbol{I}$ and $\boldsymbol{0}$ represent identity matrix and zero matrix with appropriate size, respectively. $\parallel \boldsymbol{a} \parallel$ represents 2-norm of vector $\boldsymbol{a}$.

2. ZUPT-Aided PNS

When a person is walking, the IMU fixed on the foot can obtain the foot acceleration and angular velocity information in real time, and the pedestrian positioning information can be calculated through the strapdown inertial navigation system (SINS). Due to the pedestrian velocity being relatively low and the high noise of MEMS-IMU, a simplified SINS can be defined as follows:

$$\boldsymbol{C}_{b,k}^{n} = \boldsymbol{C}_{b(k-1)}^{n}(\boldsymbol{I}_3 + \boldsymbol{\Omega}_k \Delta_t) \tag{1}$$

$$\boldsymbol{v}_k^n = \boldsymbol{v}_{k-1}^n + \left(\boldsymbol{C}_{b_k}^n \boldsymbol{f}_k^b + \boldsymbol{g}^n\right)\Delta_t \tag{2}$$

$$\boldsymbol{p}_k^n = \boldsymbol{p}_{k-1}^n + \frac{\boldsymbol{v}_k^n + \boldsymbol{v}_{k-1}^n}{2}\Delta_t \tag{3}$$

where subscripts k ($k = 1;\ 2, \ldots;\ N$) represent the sample time, Δ_t denotes the sampling period, $\boldsymbol{I}_p$ denotes p×p identity matrix, $\boldsymbol{\Omega}_k$ is the antisymmetric matrix of angular velocity measured by gyroscope, $\boldsymbol{C}_{b_k}^n$ is the attitude matrix from the body frame to the navigation frame, $\boldsymbol{g}^n = \begin{bmatrix} 0 & 0 & -g \end{bmatrix}$ represents the gravitational acceleration in the navigation frame, $\boldsymbol{v}_k^n$ and $\boldsymbol{p}_k^n$ are the velocity and the position in the navigation coordinate system at epoch k.

For foot-mounted PNS, the navigation error state transition model is a nonlinear function, the traditional Kalman filter cannot be used. Thus, the EKF is used to estimate the INS navigation error state variable, and the foot-mounted INS error state variable can be defined as:

$$\boldsymbol{X} = \begin{bmatrix} \delta\boldsymbol{p}^T & \delta\boldsymbol{v}^T & \delta\boldsymbol{\Phi}^T & \delta\boldsymbol{B}_a^T & \delta\boldsymbol{B}_g^T \end{bmatrix} \tag{4}$$

here, $\boldsymbol{X}$ is the state vector of the system. $\delta\boldsymbol{p}\quad \delta\boldsymbol{v}\quad \delta\boldsymbol{\Phi}\quad \delta\boldsymbol{B}_a\quad \delta\boldsymbol{B}_g$ are the position error, velocity error, attitude error, and zero bias error of the accelerometer and gyroscope. The dynamic error model of the INS in the discrete form can be defined as:

$$\delta\boldsymbol{X}_{k,k-1} = \boldsymbol{F}_{k,k-1}\delta\boldsymbol{X}_{k-1} + \boldsymbol{G}_{k,k-1}\boldsymbol{W}_{k-1} \tag{5}$$

where $\boldsymbol{W}_{k-1}$ represents the process noise matrix at time $k-1$, which is assumed to be zero mean Gaussian white noise. $\boldsymbol{F}_{k,k-1}$ and $\boldsymbol{G}_{k,k-1}$ are the state transition and noise gain matrices of the system state from epoch $k-1$ to k, respectively, which can be written as:

$$\boldsymbol{F} = \begin{bmatrix} \boldsymbol{I}_3 & \boldsymbol{0}_3 & \boldsymbol{0}_3 & \boldsymbol{0}_3 & -\boldsymbol{C}_b^n\Delta t \\ \Delta t\left(\boldsymbol{C}_b^n\boldsymbol{f}^b\right)\times & \boldsymbol{I}_3 & \boldsymbol{0}_3 & \boldsymbol{C}_b^n\Delta t & \boldsymbol{0}_3 \\ \boldsymbol{0}_3 & \Delta t\boldsymbol{I}_3 & \boldsymbol{I}_3 & \boldsymbol{0}_3 & \boldsymbol{0}_3 \\ \boldsymbol{0}_3 & \boldsymbol{0}_3 & \boldsymbol{0}_3 & \boldsymbol{I}_3 + \Delta t\cdot\mathrm{diag}\left(-\frac{1}{\tau_g}\right) & \boldsymbol{0}_3 \\ \boldsymbol{0}_3 & \boldsymbol{0}_3 & \boldsymbol{0}_3 & \boldsymbol{0}_3 & \boldsymbol{I}_3 + \Delta t\cdot\mathrm{diag}\left(-\frac{1}{\tau_a}\right) \end{bmatrix} \tag{6}$$

$$\boldsymbol{G} = \begin{bmatrix} \boldsymbol{0}_3 & \boldsymbol{0}_3 & \boldsymbol{0}_3 & \boldsymbol{0}_3 \\ \boldsymbol{C}_b^n\Delta t & \boldsymbol{0}_3 & \boldsymbol{0}_3 & \boldsymbol{0}_3 \\ \boldsymbol{0}_3 & \boldsymbol{C}_b^n\Delta t & \boldsymbol{0}_3 & \boldsymbol{0}_3 \\ \boldsymbol{0}_3 & \boldsymbol{0}_3 & \boldsymbol{I}_3\Delta t & \boldsymbol{0}_3 \\ \boldsymbol{0}_3 & \boldsymbol{0}_3 & \boldsymbol{0}_3 & \boldsymbol{I}_3\Delta t \end{bmatrix} \tag{7}$$

where $(\cdot)\times$ denotes the skew-symmetric matrix of a vector. $\boldsymbol{0}_p$ denotes p×p zero matrix. The error model of gyroscopes and accelerometers can be regarded as first-order Markov processes with the correlation time τ_g and τ_a.

When the foot is static, the measurement equation can be written as:

$$\boldsymbol{Z}_k^{zupt} = \boldsymbol{H}^{zupt}\boldsymbol{X}_k + v^{zupt} \tag{8}$$

where Z_k^{zupt} is a measurement vector. v^{zupt} is measurement noise matrix, which is assumed to be zero mean Gaussian white noise. H^{zupt} is measurement equation transfer matrix, which can be expressed as follows:

$$H^{\rm zupt} = \begin{bmatrix} \mathbf{0}_3 & \boldsymbol{I}_3 & \mathbf{0}_3 & \mathbf{0}_3 & \mathbf{0}_3 \end{bmatrix} \tag{9}$$

3. The Proposed Method

3.1. The Proposed Zero Velocity Detector

The two most common detection methods are acceleration measurements variance detector (AMV) and angular rate energy (ARE) detector. These detection methods judge the motion state by statistically analyzing IMU data over a period of time. However, since the output IMU data is a time series, each IMU data sample in a time window reflects the current gait state to varying degrees. In a sliding window, the weight of each sample is composed of basic constant weight and dynamic weight, we define the weight of the IMU data at the ith time as follows:

$$w_i^k = w_{i,static}^k + w_{i,dynamic}^k \qquad k \in 0, 1 \ldots . N-1 \tag{10}$$

where

$$w_{i,static}^k = \frac{(1-\lambda)^N}{N} \quad w_{i,dynamic}^k = \lambda(1-\lambda)^k \quad \sum_{k=0}^{N-1} w_i^k = 1 \tag{11}$$

where λ is the smoothing parameter. N denotes the sliding window size. w_i^k is the weight of the kth IMU data at the ith time. The sum of all sample weights in a sliding window is equal to 1. Due to the static weight being only related to the sliding window and smoothing parameters, the static weight of each sample is equal, the exponential distribution of dynamic weights can ensure that the weights of samples are different. In addition, Figure 1 shows the change trend of IMU sample data weight in a sliding window. It can be seen from Figure 1 that the weight of the sample at the current time is the largest and the weight value will decay over time, and λ determines the descending speed of the weight.

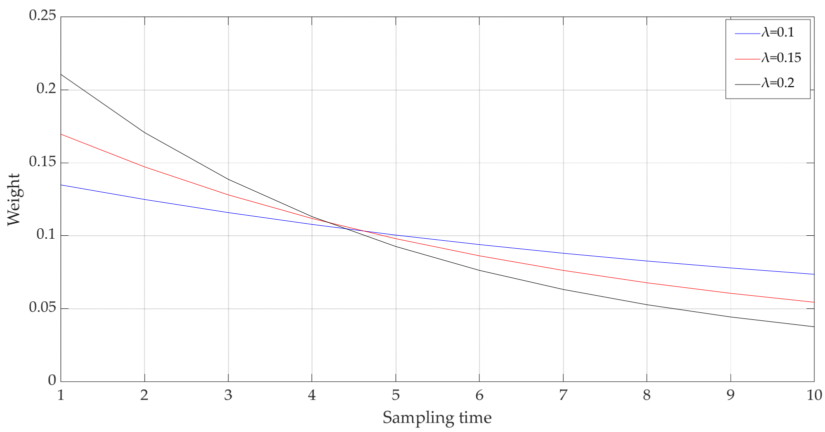

Figure 1. Weight distribution of each IMU data sample in a time window (N = 10).

So we define the following two zero-velocity detectors based on the output of the gyroscope and accelerometer:

$$T_{gro}^i = \sum_{j=0}^{N-1} w_i^k \parallel \boldsymbol{f}_i^k - \bar{\boldsymbol{f}}^i \parallel^2 \tag{12}$$

$$T_{acc}^i = \sum_{j=0}^{N-1} w_i^k \boldsymbol{\omega}_i^{k2} \tag{13}$$

where T^i_{gro} and T^i_{acc} represent two detectors with their respective thresholds λ_1 and λ_2, $\boldsymbol{f}^k_i$, $\boldsymbol{\omega}^k_i$ are the specific force and angular rate vector of the jth sample at the ith time, respectively, $\|\cdot\|$ represents 2-norm.

Combine these two detectors, Judgment is of zero velocity state:

$$C_{(i)} = \begin{cases} 1 & T^i_{gro} < \lambda_1 \& T^i_{acc} < \lambda_2 \\ 0 & others \end{cases} \tag{14}$$

If $C_{(i)}$ is equal to 1, it means that the foot is still at the current moment, otherwise, the foot is moving. Since the gait types of pedestrians are diverse, Figure 2 depicts the test statistics of the accelerometers and gyroscopes in the three gait modes. It can be seen from Figure 2 that the statistics of the accelerometers and gyroscopes are different under different gaits, so the threshold value of the proposed zero-velocity detector at different gait velocities is listed in Table 1.

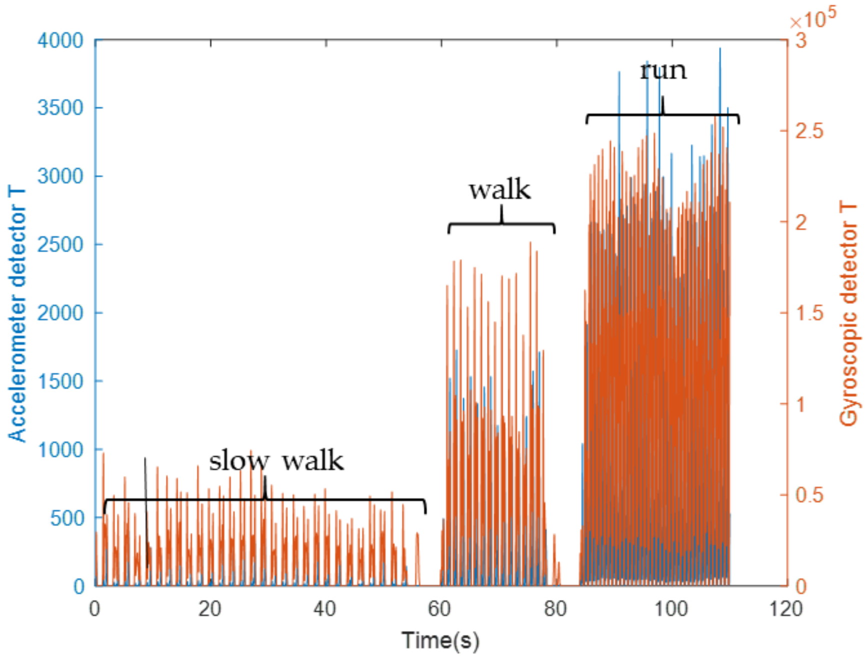

Figure 2. The test statistics of the accelerometers and gyroscopes in the three gait modes.

Table 1. The threshold of the proposed zero velocity detector at different gait velocity.

Gait Velocity (m/s)	0.4	0.49	0.75	1.09	1.3	1.7
λ_1	0.002	0.006	0.01	0.02	1.26	2.3
λ_2	10	40	110	250	1200	1850

The common traditional zero-velocity detectors use some methods to process IMU data in a time window, so the computational complexity of these zero-velocity detection algorithms is O_N. Compared with other traditional detection methods, the proposed algorithm uses the weighted method to process IMU data and calculate statistics, so the algorithm complexity is also O_N. The proposed method obtained higher positioning accuracy than the traditional methods while the computational complexity is the same.

3.2. Lateral Velocity Restrict Algorithm

When a person walks normally, the foot moves almost in the forward direction and does not move sideways, so a lateral velocity constraint algorithm can be used to restrict the accumulation of positioning errors. Since the device is installed on the foot, the forward direction of the foot is approximately the same as the y-axis of the carrier coordinate system. First, the velocity relationship between the navigation frame and the body frame is given as:

$$\boldsymbol{v}^b + \delta \boldsymbol{v}^b = \boldsymbol{C}_n^b (\boldsymbol{I}_3 + \delta \boldsymbol{\Phi}^n \times)(\boldsymbol{v}_n + \delta \boldsymbol{v}^n) \tag{15}$$

In Equation (15), $\delta \boldsymbol{\Phi}^n \times \delta \boldsymbol{v}^n \approx \mathbf{0}$, the Equation (15) can be adjusted to

$$\delta \boldsymbol{v}^b = -\boldsymbol{C}_n^b (v^n \times) \delta \boldsymbol{\Phi}^n + \boldsymbol{C}_n^b \delta v^n \tag{16}$$

Based on Equation (16), the measurement equation of lateral velocity restrict algorithm can be expressed as follows:

$$\boldsymbol{Z}_k^{lateral} = \boldsymbol{H}_k^{lateral} \boldsymbol{X}_k + \boldsymbol{v}^{lateral} \tag{17}$$

where $\boldsymbol{Z}_k^{lateral} = [0 - V_E]$ is the observation vector, $\boldsymbol{H}_k^{lateral}$ denotes the measurement matrix. $v^{lateral}$ represents the measurement noise matrix, the matrices involved are defined explicitly as

$$\boldsymbol{H}_k^{lateral} = \begin{bmatrix} \mathbf{0}_{1\times3} & \boldsymbol{A}\boldsymbol{C}_n^b & -\boldsymbol{A}\boldsymbol{C}_n^b(v^n \times) & \mathbf{0}_{1\times3} & \mathbf{0}_{1\times3} \end{bmatrix} \tag{18}$$

where $\mathbf{0}_{1\times3}$ denotes 1×3 zero matrix, $\boldsymbol{C}_n^b$ is the direction cosine matrix from the navigation frame to the body frame. $\boldsymbol{A}$ is a constant matrix and can be expressed as follows:

$$\boldsymbol{A} = \begin{bmatrix} 0 & 1 & 0 \end{bmatrix} \tag{19}$$

3.3. Step Height-Aided Altitude Correction

As shown in Figure 3, in the actual building, the height of each stair step in the building is almost the same after the actual measurement. Therefore, when pedestrians go upstairs or downstairs, the step height can be used to assist INS. The altitude measurement accuracy of the ZUPT-aided INS is reliable in a short time, so with the help of the stair step height, the pedestrian's altitude can be defined as:

$$h_i^{static} = \begin{cases} h_{i-1}^{static} + \mathrm{n}h_{stair} & 0 < h_{i,INS}^{static} - h_{i-1}^{static} - \mathrm{n}h_{stair} < th_h \\ h_{i-1}^{static} - \mathrm{n}h_{stair} & 0 < h_{i-1}^{static} - h_{i,INS}^{static} - \mathrm{n}h_{stair} < th_h \end{cases} \tag{20}$$

where h_i^{static} and h_{i-1}^{static} are the updated altitude of ith and $(i-1)$th step, h_{stair} is the measured step height, $h_{i,INS}^{static}$ is the altitude of i step obtained through INS, th_h is the preset limit threshold, which is set to $\frac{h_{stair}}{2}$.

Figure 3. Height of stair steps in buildings.

4. Results

4.1. Experimental Setup

Figure 4 shows the system framework of the proposed 3D positioning scheme. The 2D plane positioning is carried out by the improved zero velocity detector and lateral velocity restrict algorithm. The stair step height is used to limit the altitude positioning error caused by INS. The data of the experiment is available for download here: https://github.com/laotouyu123/Electronics_data_set.git, accessed on 24 November 2022.

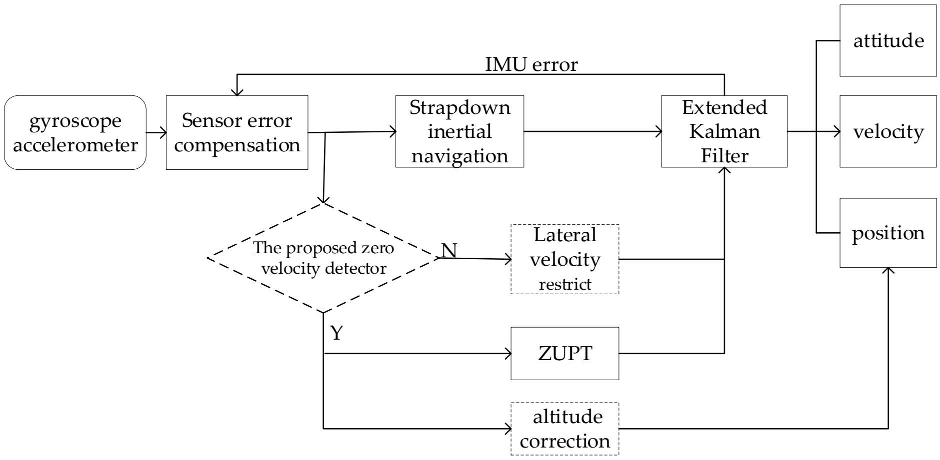

Figure 4. Flow chart of the proposed method.

As illustrated in Figure 5, the MTI-710 device produced by a Dutch company was mounted on the shoe, which includes a three-axis gyroscope, accelerometer, and magnetometer. The observations of all sensors are transmitted to a laptop. In the experiment, only the data from three-axis accelerometers and gyroscopes are used to evaluate algorithm performance, the IMU sampling rate of the system is set to 100. The main performance parameters of the sensor are shown in Table 2.

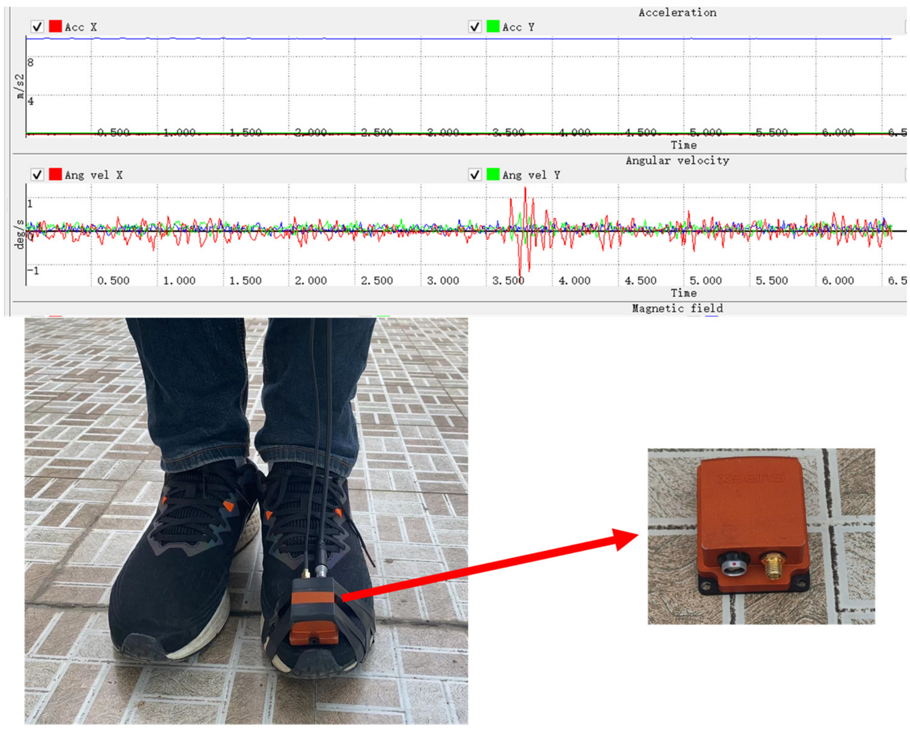

Figure 5. Experimental hardware platform.

Table 2. Performance parameter of MTI-710.

Sensor Type	Parameter	Value
Accelerometer	Full range Noise density Bias stability	18 g 80 $\mu g/Hz^{1/2}$ 40 μg
Gyroscope	Full range Noise density Bias stability	$625°/s$ $0.01°/s/Hz^{1/2}$ $10°/h°/s$

4.2. Zero Velocity Detection Experiment

The accuracy of the zero velocity detector has an important impact on position estimation. In the actual test, the closed position error is often chosen as a performance metric. In this section, an experimenter moves along a rectangular path with three gait types (slow walk, walk, run), and finally returns to the original position. The INS closed position error is calculated by using MAG, GLRT, and improved zero velocity detection.

Figure 6 depicts the trajectory estimated using three different zero velocity detectors. As can be seen from the trajectory results in Figure 6, under slow walk mode, the performance of the three zero velocity detectors is satisfactory. However, as for walk and run mode, the positioning results calculated by the proposed method are better than those observed by the other two methods. The MAG detector only uses the accelerometer amplitude to detect the zero velocity range, so its performance is the worst. The final endpoint of the trajectory obtained by using the proposed zero velocity detector in the three motion modes is obviously close to the starting point.

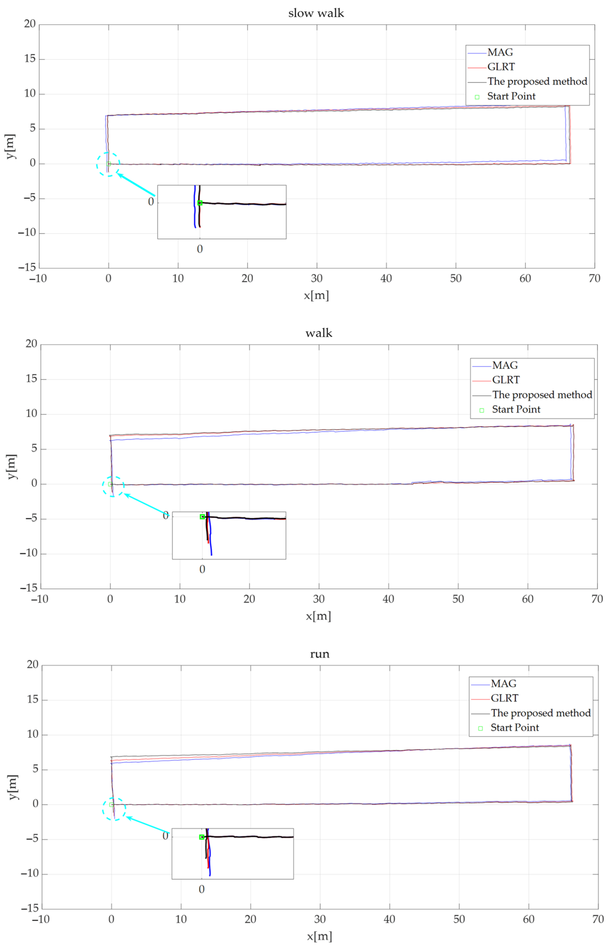

Figure 6. Trajectories obtained by using different zero velocity detectors under three motion modes.

Table 3 summarizes the closure position error results of each zero velocity detection method. As shown in Table 3, the closed error observed by the proposed method is obviously lower than MAG and GLRT. Compared with the MAG, the closed position error observed by using the proposed method is decreased by 4.14%, 36.96%, and 47.83%, respectively, in three motion modes. Compared with the GLRT, the average position error calculated by using the proposed method is decreased by 1.66%, 7.19%, and 34.55%, respectively.

Table 3. Closure position error of zero velocity detection experiment.

Motion Mode	Method	Closure Error (m)	Closure Error/ Trajectory Length
Slow walk (0.5 m/s)	MAG	1.24	0.83%
	GLRT	1.21	0.81%
	The proposed method	1.19	0.8%
Walk (1 m/s)	MAG	1.84	1.23%
	GLRT	1.25	0.84%
	The proposed method	1.16	0.78%
Run (1.5 m/s)	MAG	2.07	1.39%
	GLRT	1.65	1.11%
	The proposed method	1.08	0.72%

4.3. The 2D Plane Positioning Experiment under Mixed Gait

A mixed gait experiment is used to evaluate the two-dimensional plane positioning accuracy of the proposed algorithm. As shown in Figure 7, first, the pedestrian walked along a rectangular path of 174.4 m, then ran back to the start point. The reference track can be measured by high-precision real-time kinematic (RTK) equipment produced by U-blox. The tracking trajectory by the proposed method was compared with those by ZUPT-aided INS and the combination scheme of INS calculation and step length estimation models [26].

Figure 7. The experiment environment.

Figure 8 shows the motion trajectory estimated by different methods. As shown in Figure 8, since the designed motion trajectory contains three gaits, the proposed method sets a different threshold for different gaits and uses the improved zero velocity detection algorithm and lateral velocity restrict algorithm, so the motion trajectory calculated using the proposed method is obviously better than the traditional ZUPT-aided INS. Although the step length model and heading angle are used to calculate the pedestrian position, due to the error of step size estimation and heading drift, the position trajectory estimated by the integrated method obviously deviates from the real trajectory.

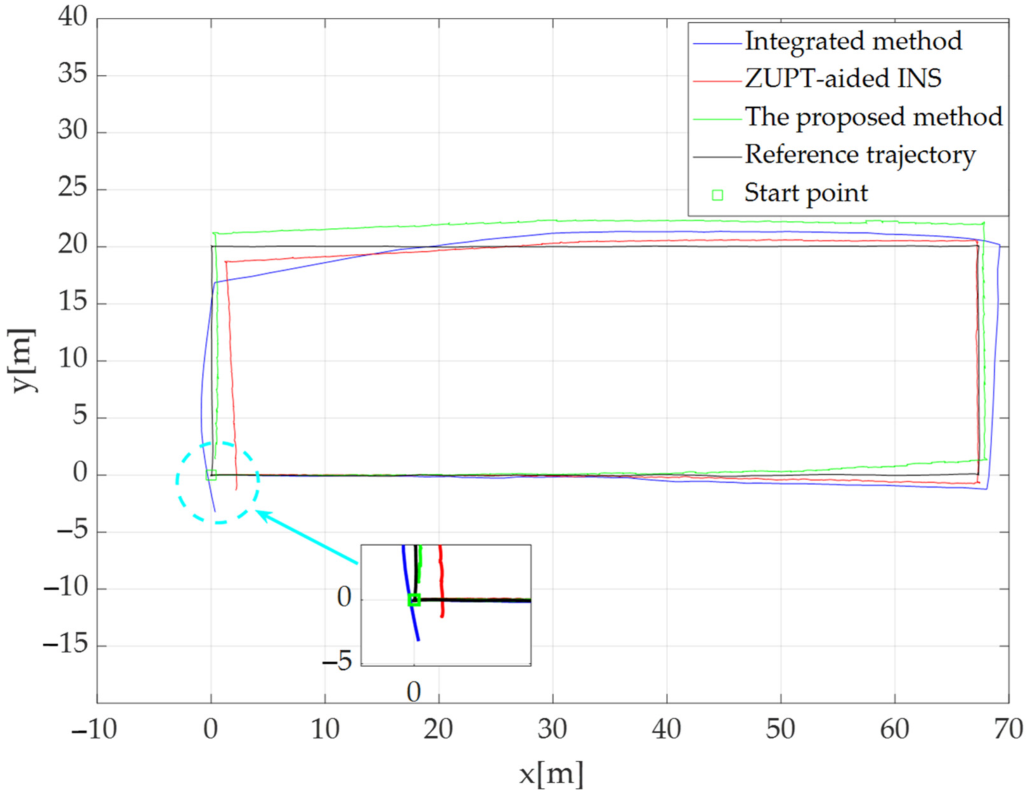

Figure 8. The 2D motion trajectory estimated by different methods.

From the closure error statistics data in Table 4, it can be seen that the closure errors obtained by the three methods are 3.25 m, 2.54 m, and 1.52 m, respectively, compared with the traditional ZUPT-aided INS, the closure error calculated using the proposed algorithm is reduced by 53.24%. Compared with the integrated method, the closing error of the proposed algorithm is decreased by 40.16%. Therefore, the proposed method can effectively reduce the positioning error of pedestrian navigation.

Table 4. Position error of mixed gaits experiment.

Method	Closure Error (m)	Closure Error/Trajectory Length
ZUPT-aided INS	3.25	1.86%
The integrated method	2.54	1.45%
The proposed method	1.52	0.87%

4.4. Altitude Experiment

A multi-floor experiment is designed to test the height positioning accuracy of the algorithm. Figure 9 shows the experimental site of the indoor altitude experiment. As shown in Figure 9, a pedestrian equipped with the equipment walks from the first floor to the sixth floor of the building, then returns to the first floor from the seventh floor, and finally returns to the original position. The height of each floor is measured with high-precision measuring equipment.

Figure 9. Experimental site of indoor altitude experiment.

Figure 10 shows the altitude test results by ZUPT-aided INS (blue line), step-aided INS algorithm (red line). As shown in Figure 10, although the altitude positioning of the ZUPT-aided INS can reflect the altitude change of pedestrians, the estimated altitude obviously deviates from the real floor height as time increases. The proposed scheme can use steps well to assist the INS, which effectively reduces error accumulation.

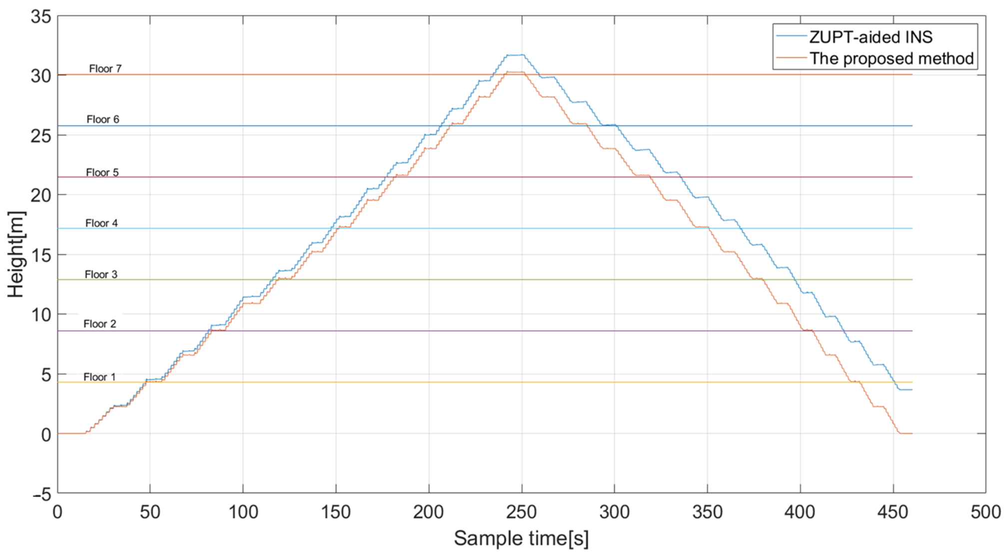

Figure 10. The altitude estimated by different methods.

Table 5 lists the maximum altitude positioning error and average position error of different methods. It can be seen from Table 5 that the maximum error of the traditional ZUPT-aided INS and the proposed method are 1.65 m and 0.95 m, and the average errors are 0.19 m and 0.12 m, compared with traditional ZUPT- aided INS, the maximum error of the proposed method is decreased by 88.49%, and the average position error is reduced by 87.37%.

Table 5. Altitude error of different methods.

Method	Maximum Altitude Error (m)	Average Altitude Error (m)
ZUPT-aided INS	1.65	0.95
The proposed method	0.19	0.12

5. Conclusions

In this article, we proposed a novel 3D pedestrian positioning scheme based on low-cost IMU. First, according to the motion characteristics of pedestrians, an improved zero-velocity detector is designed to detect the zero-velocity interval of pedestrians.The proposed zero-velocity detector is mainly composed of an accelerometer detector and gyroscope detector and can set different threshold values for different motion modes. The proposed lateral velocity restrict algorithm can effectively limit the east velocity error in the carrier coordinate system. When pedestrians are going upstairs, the stair step/INS fusion framework can effectively improve the altitude positioning performance, experimental results demonstrate that the proposed method achieves better positioning performance than other traditional algorithms.

Since pedestrian movement is random and complex in the actual environment, the proposed lateral velocity restrict algorithm can only be applied to some simple gait patterns, and the performance of the algorithm is not satisfactory in complex gait patterns such as lateral walking. Future work will focus on solving the positioning problem in complex motion mode and the design of fault-detection of the positioning approach.

Author Contributions: Conceptualization, J.J., D.X.; methodology, J.J., D.X. and J.W.; software, D.X.; validation, J.J. and D.X.; formal analysis, J.J., D.X.; investigation, J.J. and D.X.; resources, J.J. and D.X.; writing—original draft preparation, J.J. and D.X.; writing—review and editing, J.J., D.X., P.Y., Z.Y., J.W. and Y.L.; visualization, J.W.; supervision, J.W. and D.X.; project administration, P.Y.; funding acquisition, J.J. All authors have read and agreed to the published version of the manuscript.

Funding: This research was funded by the National Key Research and Development Program of China (2018YFB0505200 and 2018YFB0505201), the Fundamental Research Funds for the Central Universities (2042018kf0253).

Data Availability Statement: Not applicable.

Acknowledgments: Thank you very much for the equipment support of Jinguang Jiang's research group, for his driving experiment for this research, and for the technical support of Peihui Yan, Jiaji Wu, Ziyan Yu, and Yuying Li.

Conflicts of Interest: The authors declare no conflict of interest.

Abbreviations

The commonly used abbreviations in this manuscript are summarized as follows:

PNS	pedestrian navigation system
WSN	Wireless Sensor Network
GNSS	Global Navigation Satellite System
WIFI	Wireless Fidelity
IMU	inertial measurement unit
INS	inertial navigation system
ZUPT	zero velocity update algorithm
ARE	angular rate measurement energy test
GLRT	generalized likelihood ratio test
3D	three-dimensional
2D	two- dimensional
SINS	strapdown inertial navigation system
EKF	extended Kalman filter

References

1. Rantakokko, J.; Rydell, J.; Stromback, P.; Handel, P.; Callmer, J.; Tornqvist, D.; Gustafsson, F.; Jobs, M.; Gruden, M. Accurate and reliable soldier and first responder indoor positioning: Multisensor systems and cooperative localization. *IEEE Wirel. Commun.* **2011**, *18*, 10–18. [CrossRef]
2. Trkov, M.; Chen, K.; Yi, J.; Liu, T. Inertial Sensor-Based Slip Detection in Human Walking. *IEEE Trans. Autom. Sci. Eng.* **2019**, *16*, 1399–1411. [CrossRef]

3. Li, D.; Gu, Y.; Kamijo, S. Pedestrian Positioning in Urban Environment by Integration of PDR and Traffic Mode Detection. In Proceedings of the 20th IEEE International Conference on Intelligent Transportation Systems (ITSC), Yokohama, Japan, 16–19 October 2017.
4. Hui, F.; Qin, F. Influence of Inertial Sensor Errors on GNSS/INS Integrated Navigation Performance. In Proceedings of the 8th International Conference on Measuring Technology and Mechatronics Automation (ICMTMA), Macau, China, 11–12 March 2016; pp. 347–351.
5. Shu, Y.; Huang, Y.; Zhang, J.; Coue, P.; Cheng, P.; Chen, J.; Shin, K.G. Gradient-Based Fingerprinting for Indoor Localization and Tracking. *IEEE Trans. Ind. Electron.* **2016**, *63*, 2424–2433. [CrossRef]
6. Kanaris, L.; Kokkinis, A.; Liotta, A.; Stavrou, S. Fusing Bluetooth Beacon Data with Wi-Fi Radiomaps for Improved Indoor Localization. *Sensors* **2017**, *17*, 812. [CrossRef] [PubMed]
7. Sugano, M.; Kawazoe, T.; Ohta, Y.; Murata, M. Indoor localization system using RSSI measurement of wireless sensor network based on ZigBee standard. In Proceedings of the 6th IASTED International Conference on Wireless and Optical Communica-tions, Banff, AB, Canada, 3–5 July 2006.
8. Javadi, S.H.; Moosaei, H.; Ciuonzo, D. Learning Wireless Sensor Networks for Source Localization. *Sensors* **2019**, *19*, 635. [CrossRef]
9. Jondhale, S.; Rajagopal, M.; Lloret, J. *Received Signal Strength Based Target Localization and Tracking Using Wireless Sensor Networks*; Springer: Berlin, Germany, 2022.
10. Brigante, C.M.N.; Abbate, N.; Basile, A.; Faulisi, A.C.; Sessa, S. Towards Miniaturization of a MEMS-Based Wearable Motion Capture System. *IEEE Trans. Ind. Electron.* **2011**, *58*, 3234–3241. [CrossRef]
11. Jimenez Ruiz, A.R.; Seco Granja, F.; Prieto Honorato, J.C.; Guevara Rosas, J.I. Accurate Pedestrian Indoor Navigation by Tightly Coupling Foot-Mounted IMU and RFID Measurements. *IEEE Trans. Instrum. Meas.* **2012**, *61*, 178–189. [CrossRef]
12. Skog, I.; Handel, P.; Nilsson, J.-O.; Rantakokko, J. Zero-Velocity Detection-An Algorithm Evaluation. *IEEE Trans. Biomed. Eng.* **2010**, *57*, 2657–2666. [CrossRef] [PubMed]
13. Nilsson, J.-O.; Skog, I.; Handel, P.; Hari, K.V.S.; IEEE. Foot-mounted INS for Everybody—An Open-source Embedded Implementation. In Proceedings of the IEEE/ION Position Location and Navigation Symposium (PLANS), Myrtle Beach, SC, USA, 23–26 April 2012; pp. 140–145.
14. Wang, Q.; Guo, Z.; Sun, Z.; Cui, X.; Liu, K. Research on the Forward and Reverse Calculation Based on the Adaptive Zero-Velocity Interval Adjustment for the Foot-Mounted Inertial Pedestrian-Positioning System. *Sensors* **2018**, *18*, 1642. [CrossRef] [PubMed]
15. Skog, I.; Nilsson, J.-O.; Handel, P. Evaluation of Zero-Velocity Detectors for Foot-Mounted Inertial Navigation Systems. In Proceedings of the International Conference on Indoor Positioning and Indoor Navigation (IPIN), Zurich, Switzerland, 15–17 September 2010.
16. Wang, P.; Pan, K.; Ren, M.; Zhang, X. Indoor Personal Navigation System Based on Zero Velocity Detection of Pseudo Adaptive Threshold. *J. Beijing Univ. Technol.* **2015**, *41*, 1308–1313.
17. Niu, X.; Li, Y.; Kuang, J.; Zhang, P. Data Fusion of Dual Foot-Mounted IMU for Pedestrian Navigation. *IEEE Sens. J.* **2019**, *19*, 4577–4584. [CrossRef]
18. Ju, H.; Lee, J.H.; Park, C.G.; Lee, C.S.; Seol, D.M. A Waist-mounted Pedestrian Dead Reckoning System by Fusing Integration and Parametric Approaches. *J. Inst. Control Robot. Syst.* **2019**, *25*, 334–339. [CrossRef]
19. Wagstaff, B.; Kelly, J. LSTM-Based Zero-Velocity Detection for Robust Inertial Navigation. In Proceedings of the 9th International Conference on Indoor Positioning and Indoor Navigation (IPIN), Nantes, France, 24–27 September 2018.
20. Zhao, T.; Ahamed, M.J. Pseudo-Zero Velocity Re-Detection Double Threshold Zero-Velocity Update (ZUPT) for Inertial Sensor-Based Pedestrian Navigation. *IEEE Sens. J.* **2021**, *21*, 13772–13785. [CrossRef]
21. Wang, Q.; Liu, K.; Sun, Z.; Cai, M.; Cheng, M. Research on the Heading Calibration for Foot-Mounted Inertial Pedestrian-Positioning System Based on Accelerometer Attitude. *Electronics* **2019**, *8*, 1405. [CrossRef]
22. Chen, Z.; Pan, X.; Wu, M.; Zhang, S.; Wang, M. A Novel Adaptive Zero-Velocity Detector for Inertial Pedestrian Navigation Based on Optimal Interval Estimation. *IEEE Access* **2020**, *8*, 191888–191900. [CrossRef]
23. Li, Y.; Zhuang, Y.; Zhang, P.; Lan, H.; Niu, X.; El-Sheimy, N. An improved inertial/wifi/magnetic fusion structure for indoor navigation. *Inf. Fusion* **2017**, *34*, 101–119. [CrossRef]
24. Zeng, Q.; Wang, J.; Meng, Q.; Zhang, X.; Zeng, S. Seamless Pedestrian Navigation Methodology Optimized for Indoor/Outdoor Detection. *IEEE Sens. J.* **2018**, *18*, 363–374. [CrossRef]
25. Ji, M.; Liu, J.; Xu, X.; Lu, Z. The Improved 3D Pedestrian Positioning System Based on Foot-Mounted Inertial Sensor. *IEEE Sens. J.* **2021**, *21*, 25051–25060. [CrossRef]
26. Weinberg, H. Using the ADXL202 in pedometer and personal navigation applications. *Analog Devices-602 Appl. Note* **2002**, *2*, 1–6.